Single-molecule correlated chemical probing of RNA

Philip J. Homan[a], Oleg V. Favorov[b], Christopher A. Lavender[a], Olcay Kursun[c], Xiyuan Ge[a], Steven Busan[a], Nikolay V. Dokholyan[d], and Kevin M. Weeks[a,1]

Departments of [a]Chemistry, [b]Biomedical Engineering, and [d]Biochemistry and Biophysics, University of North Carolina, Chapel Hill, NC 27599; and [c]Department of Computer Engineering, Istanbul University, Avcilar, Istanbul 34320, Turkey

Edited by Ignacio Tinoco, Jr., University of California, Berkeley, CA, and approved August 11, 2014 (received for review April 21, 2014)

Complex higher-order RNA structures play critical roles in all facets of gene expression; however, the through-space interaction networks that define tertiary structures and govern sampling of multiple conformations are poorly understood. Here we describe single-molecule RNA structure analysis in which multiple sites of chemical modification are identified in single RNA strands by massively parallel sequencing and then analyzed for correlated and clustered interactions. The strategy thus identifies RNA interaction groups by mutational profiling (RING-MaP) and makes possible two expansive applications. First, we identify through-space interactions, create 3D models for RNAs spanning 80–265 nucleotides, and characterize broad classes of intramolecular interactions that stabilize RNA. Second, we distinguish distinct conformations in solution ensembles and reveal previously undetected hidden states and large-scale structural reconfigurations that occur in unfolded RNAs relative to native states. RING-MaP single-molecule nucleic acid structure interrogation enables concise and facile analysis of the global architectures and multiple conformations that govern function in RNA.

spectral clustering | structure refinement | motif discovery | dimethyl sulfate

RNA plays a central role in gene expression and regulation. These functions are mediated by tiered levels of information: The simplest is the primary sequence, and the most complex is the higher-order structure that governs interactions with ligands, proteins, and other RNAs (1, 2). Many RNAs can form more than one stable structure, and these distinct conformations often have different biological activities (3, 4). Currently, the rate of describing new RNA sequences vastly exceeds abilities to examine their structures.

Here we characterize through-space interactions and multiple conformations in single RNAs by melding chemical probing and massively parallel sequencing. Because massively parallel sequencing reports the sequences of single templates, each read is fundamentally a single-molecule observation (5). We first modified RNA with a reagent that is sensitive to the underlying RNA structure and then detected multiple adducts in individual RNA strands (Fig. 1). Chemical adducts were detected as sequence mutations based on their ability to induce efficient misreading of the template nucleotide by a reverse transcriptase enzyme, an approach called mutational profiling, or MaP (6). Single-molecule probing data were used in two distinct ways: to detect correlated RNA modifications reflecting higher-order through-space interactions (Fig. 1*A*) and to examine multiple conformations in single in-solution ensembles (Fig. 1*B*).

Results and Discussion

Multisite Dimethyl Sulfate Reactivity with RNA. We used dimethyl sulfate (DMS) to probe the structures of three RNAs: the *Escherichia coli* thiamine pyrophosphate (TPP) riboswitch (79 nt) (7), the *Tetrahymena* group I intron P546 domain (160 nt) (8), and the *Bacillus stearothermophilus* RNase P catalytic domain (265 nt) (9). RNAs were selected to illustrate distinct RNA folding features and to emphasize increasingly difficult analysis challenges. The TPP riboswitch binds the TPP ligand to function in gene regulation. The P546 domain has a U-shaped structure stabilized by a long-range tertiary interaction spanning roughly 45 base pairs. The RNase P domain is among the largest RNAs for which automated modeling has been pursued. DMS forms adducts at the N1 position of adenosine and N3 position of cytosine (Fig. 2*A*). We optimized conditions to yield multiple modifications in an RNA strand without disrupting native RNA folding (Fig. S1). RNA samples were treated with 170 mM DMS in 10 mM Mg^{2+} and 300 mM cacodylate buffer at pH 7 for 6 min. The reactions were quenched by addition of excess 2-mercaptoethanol. Cytosine and adenosine nucleotides were methylated with equal efficiencies, and ∼12% of nucleotides were modified under these conditions (Fig. 2*B*).

We detected sites of DMS methylation directly as adduct-induced mutations in the full-length cDNAs generated during reverse transcription (Fig. 1). We visualized the overall reactivity patterns for each RNA in 2D mutation frequency profiles (Fig. 3*B*). Comparison with the high-resolution structures for these RNAs (7–9) showed that nucleotides modified at high levels were those not involved in base pairing or tertiary interactions (Fig. 3*C*). As expected, nucleotide modification was dependent on reagent concentration, reaction time, and the stability of the RNA structure (Fig. S2). The observed high mutation frequencies over background allowed DMS-induced mutations to be analyzed without the requirement for background correction (Fig. 3*B*).

For the TPP riboswitch, the P546 domain, and the RNase P domain, averages of two, five, and seven adducts were detected in each sequencing read, respectively (Fig. 3*A*). Approximately 15% of the single-stranded A and C nucleotides in each RNA

Significance

RNA molecules function as the central conduit of information transfer in biology. To do this, they encode information both in their sequences and in their higher-order structures. Understanding the higher-order structure of RNA remains challenging. In this work we devise a simple, experimentally concise, and accurate approach for examining higher-order RNA structure by converting widely used massively parallel sequencing into an easily implemented single-molecule experiment for detecting through-space interactions and multiple conformations. We then use this experiment to analyze higher-order RNA structure, detect biologically important hidden states, and refine accurate three-dimensional structure models.

Author contributions: P.J.H., O.V.F., C.A.L., and K.M.W. designed research; P.J.H. performed research; S.B. and N.V.D. contributed new analytic tools; P.J.H., O.V.F., C.A.L., O.K., X.G., S.B., N.V.D., and K.M.W. analyzed data; and P.J.H., O.V.F., C.A.L., and K.M.W. wrote the paper.

Conflict of interest statement: The authors have applied for a provisional patent on elements of this work.

This article is a PNAS Direct Submission.

Data deposition: The sequences reported in this paper have been deposited in the National Center for Biotechnology Information Sequence Read Archive (accession no. SRP046153).

[1]To whom correspondence should be addressed. Email: weeks@unc.edu.

This article contains supporting information online at www.pnas.org/lookup/suppl/doi:10.1073/pnas.1407306111/-/DCSupplemental.

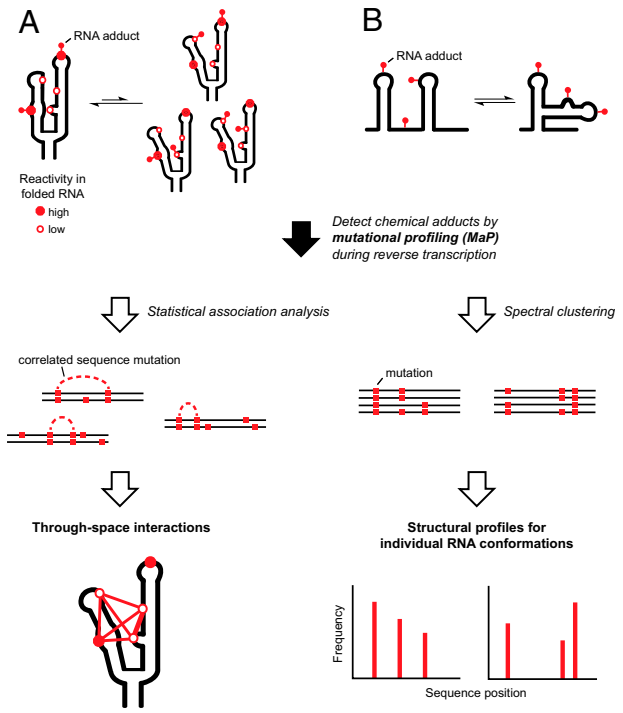

Fig. 1. Single-molecule RNA structure analysis by massively parallel sequencing. (*A*) RNA molecules experience local structural variations and "breathing" in which nucleotides become reactive to a chemical probe in a correlated way. Statistical association analysis is used to detect and quantify the strengths of these interdependencies. (*B*) RNA molecules can adopt multiple conformations in solution. Spectral clustering analysis, based on similarity of nucleotide reactivity patterns, can be used to separate data on individual RNA strands into different conformations.

were modified by DMS, comparable to the level of modification of free nucleotides under these conditions (Fig. 2). Because multiple chemical modification events were detected in sequencing reads of single RNA strands, we could quantify correlated interdependencies in reactivity. Nucleotides modified in a correlated fashion comprise RNA interaction groups, or RINGs. The correlated reactivities were measured by mutational profiling (MaP) (6), yielding a RING-MaP experiment.

Through-Space RNA Interactions Detected by Statistical Association Analysis. Nucleotides involved in through-space interactions will show correlated chemical reactivities, reflective of a "breathing" mechanism in which an RNA nucleotide becomes transiently accessible for modification. This breathing mechanism suggests that correlated probing will be selective for transient, dynamic interactions rather than static structural differences (Fig. 1*A*). We used a two-part strategy to identify reactive nucleotide pairs with statistically significant correlations and to quantify the strengths of these correlations. The interdependencies for DMS reactivities for any two positions in a single RNA strand were first evaluated using a χ^2 test. The strength of the interaction between each pair of correlated nucleotides was then quantified using Pearson's phi metric.

RINGs for the TPP riboswitch, P546 intron domain, and RNase P RNAs (Fig. 3*C*) include nucleotides known to interact based on high-resolution structures (7–9). For example, correlated positions in the TPP riboswitch correspond to nucleotides involved in a docking interaction between the L5 loop and P3 helix and in formation of the ligand-binding pocket. In the P546 domain, correlated modifications were observed at nucleotides in the L5b loop and P6a helix docking interaction, within the J5 hinge region, and throughout the lengths of the P5a and P5b helices. In the RNase P RNA, RINGs report tertiary interactions between the L5 and L15.1 loops and in the structural core. We also observed a second set of interactions in the RNase P P19 element.

RINGs Report Higher-Order and Tertiary RNA Interactions. We evaluated differences in the tertiary interactions, as reported by RINGs, under different solution conditions or in mutant RNAs. In the presence of Mg^{2+}, the P546 domain forms a U-shaped structure in which a tetraloop–receptor interaction forms between L5b and P6a and the J5 region acts as a hinge (10, 11). These interactions were correctly reported by multiple correlated chemical modifications in these structural elements (Fig. 4*A*). Disruption of this tertiary structure by folding the RNA in the absence of Mg^{2+} eliminated the majority of observed interactions (Fig. 4*B*).

The tertiary structure of the P546 domain can also be perturbed by mutations in the P6a helix and in the J5 hinge. Mutation of the C223–G250 base pair in the P6a helix to A–U disrupts the L5–P6a interaction (10). RING analysis of this mutant showed that the correlation between L5 and P6b was lost and that other parts of the RNA also underwent significant reconfiguration. Interactions involving the hinge seemed to be strengthened and more and stronger correlations were observed within the helical domains of P5a and P5b (Fig. 4*C*).

Mutations that result in base pairing of nucleotides in the J5 hinge likely yield a linear conformation for the P546 domain (11). RING analysis of the J5 mutant showed the expected loss in correlated nucleotides within the J5 region and consequently the loss of the L5b–P6a interaction (Fig. 4*D*). The correlations among nucleotides in the P5b helix were strengthened in this mutant relative to those in observed in the wild-type RNA, but no changes were observed in correlations among nucleotides in the P5a helix. This analysis of P546 domain demonstrated that RINGs accurately reflect structural interactions in a large RNA molecule at nucleotide resolution.

Detection of Multiple and Hidden RNA Conformations. In the RING-MaP approach, each RNA strand is sequenced independently by massively parallel sequencing. RNA strands of different conformations will tend to exhibit distinct groups of coreactive

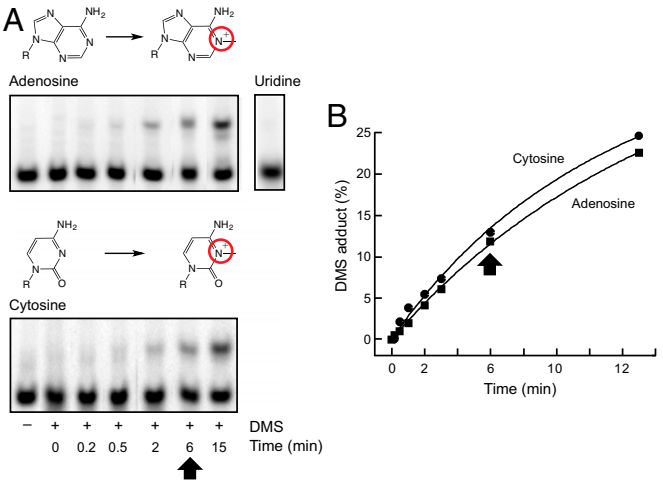

Fig. 2. Efficient DMS adduct formation at the base-pairing faces of adenosine and cytosine. (*A*) Reaction of nucleotides with 170 mM DMS in 300 mM cacodylate (pH 7) monitored by gel electrophoresis. (*B*) Time course of DMS reaction with adenosine and cytosine. Unconstrained nucleotides react to form methyl adducts with ~12% efficiency in 6 min (arrow).

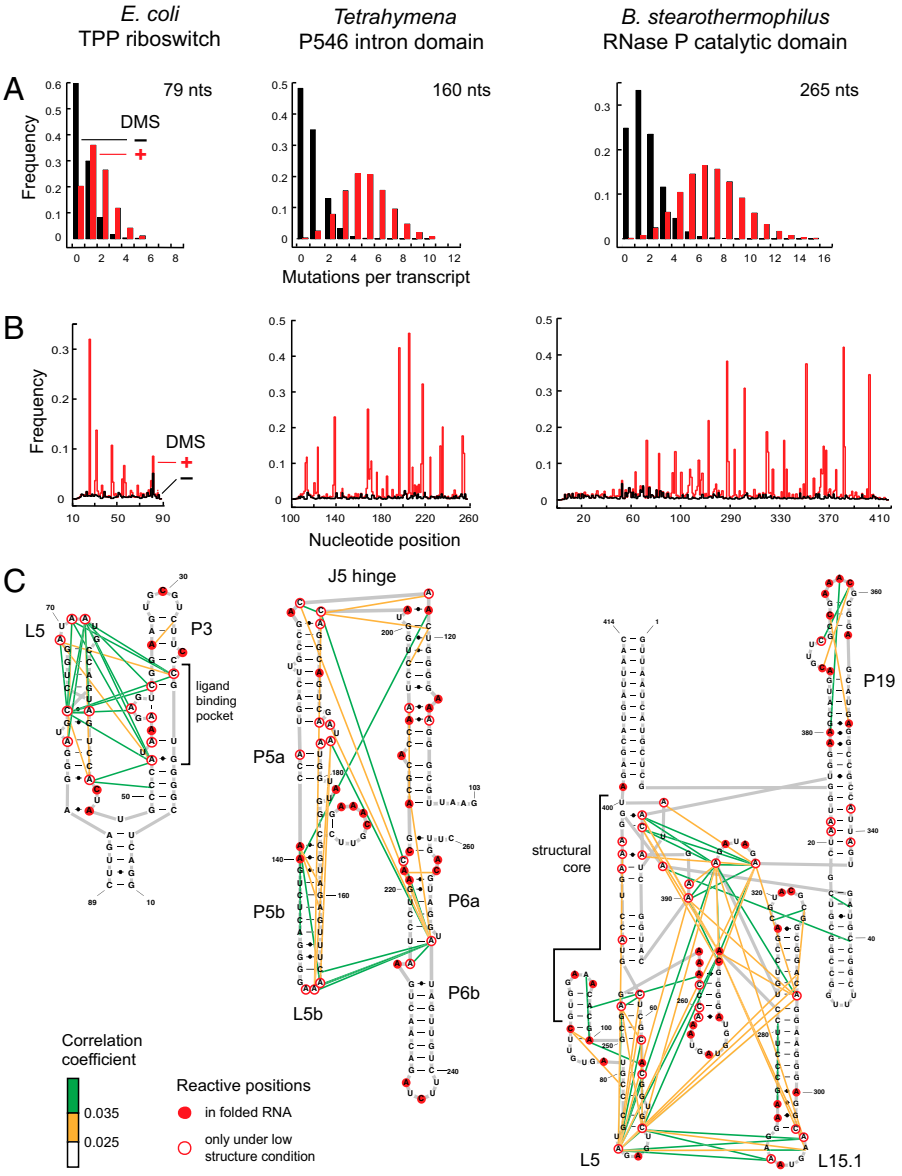

Fig. 3. RING analysis of RNA structure. (*A*) Number of mutations per transcript detected by reverse transcription with (red) and without (black) DMS modification. (*B*) DMS modification-induced mutation frequencies as a function of nucleotide position. Data from DMS-treated samples are shown in red and no-reagent controls are black. (*C*) RINGs for the TPP riboswitch, P546 domain, and RNase P RNAs showing strong (green) and moderate (yellow) correlations. Correlations occur between positions that are reactive in the native structure (filled red circles) or become reactive during "breathing" motions (open circles). Correlation coefficients of 0.025 and 0.035 correspond to median 2.5- and 2.8-fold increases, respectively, in the probability of mutation at one nucleotide owing to mutation of a second nucleotide. Secondary structures are drawn to approximate relative helical orientations in 3D space, based on known structures (7–9).

nucleotides (Fig. 1*B*). Such groups can be detected by spectral clustering and will be reflective of distinct, relatively stable individual structures in solution. Spectral clustering produces an objective estimate of the number of clusters and therefore the number of conformations adopted by a particular RNA in solution. Spectral clustering analysis of the modification data obtained on the TPP riboswitch and RNase P RNAs indicated that each RNA formed multiple distinct conformations under the conditions used in our probing experiments (Fig. S3).

RINGs identified for the TPP riboswitch with saturating ligand revealed interactions in the L5–P3 docked structure and in the ligand-binding pocket (Fig. 5*A*). There were significantly fewer internucleotide tertiary interactions in the absence of TPP ligand than in its presence; however, specific interactions in J2–4 were still observed (Fig. 5*B*). Spectral clustering revealed that both the saturating-ligand and no-ligand RNAs are composite states with constituent major and minor conformations (Fig. 5 *C* and *D*). The minor cluster in the saturating-ligand RNA is characterized by increased DMS reactivities at precisely the positions that became reactive when no ligand was bound (Fig. 5 *A* and *C*, open circles). Therefore, even under saturating-ligand conditions, the TPP riboswitch RNA samples conformations characteristic of both ligand-bound and unbound states. In the absence of ligand, the major cluster has a DMS reactivity pattern similar to the less structured state in the presence of ligand. In contrast, the minor cluster detected in the absence of ligand has reduced DMS reactivities precisely in the thiamine-binding pocket, suggestive of a conformation that is more highly structured than that of the major cluster (Fig. 5 *B* and *D*). We infer that, in the absence of ligand, the riboswitch thiamine-binding pocket samples a "hidden" prefolded structure similar to that formed upon ligand binding.

We then probed the TPP riboswitch RNA in the presence of subsaturating ligand concentrations [200 nM TTP; K_d ~50–200 nM (12)]. Clustering analysis of the chemical reactivity data produced three well-defined clusters in the ratio of 1:1:1.2 (Fig. S3) corresponding to (*i*) the fully folded, ligand-bound state, (*ii*) the state in which the ligand-binding pocket is structured but the rest of the RNA shows weak internucleotide interactions, and (*iii*) the relatively unstructured state with only a few interacting nucleotides (Fig. S4). Each of these clusters corresponds to states identified previously in either the saturating ligand or no-ligand RNAs. Spectral clustering analysis thus identified

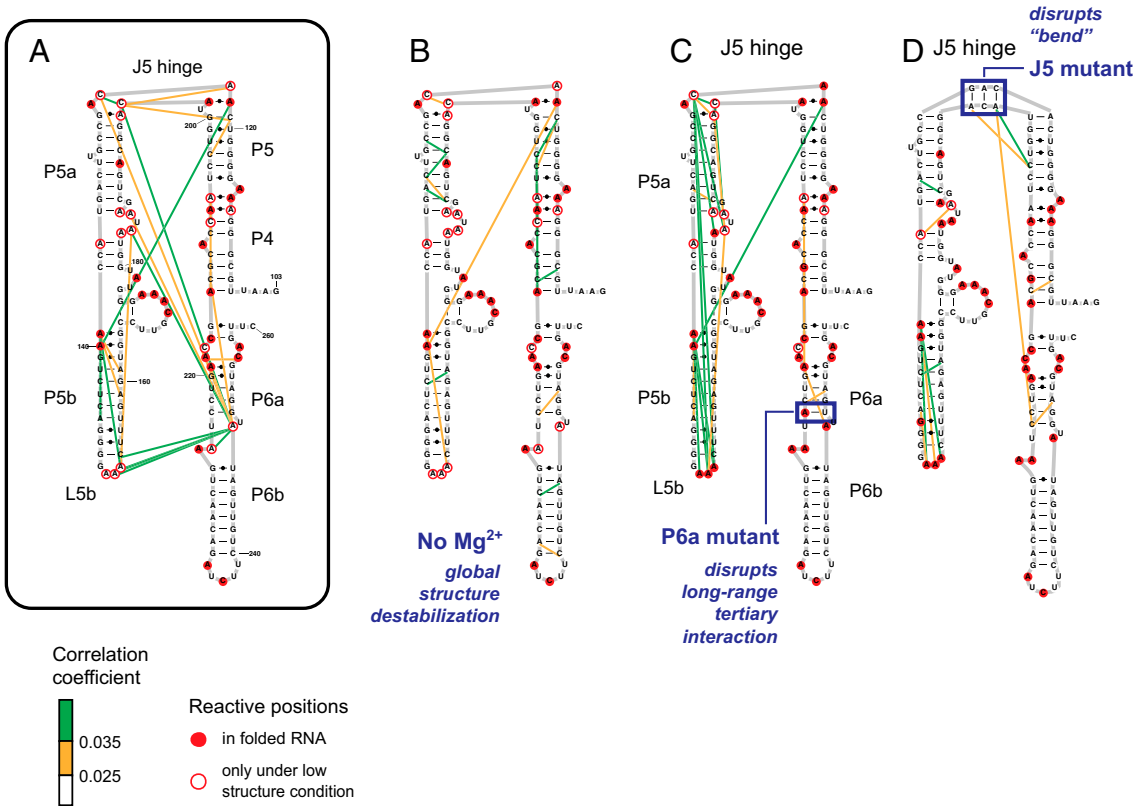

Fig. 4. RINGs report the tertiary structure of the P546 domain and mutation-induced structural changes. Strong and medium internucleotide correlations are shown with green and yellow lines, respectively. (*A*) RINGs in the P546 domain folded in the presence of Mg^{2+}. (*B*) RINGs in the P546 domain in the absence of Mg^{2+}. RINGs in the (*C*) P6a and (*D*) J5 hinge mutants. For clarity, *A* is reproduced from to Fig. 3*C*.

multiple distinct conformations from a single in-solution RNA ensemble, including a previously uncharacterized state in which the ligand-binding pocket is prefolded. This partially folded state is likely important for recognition of the TPP ligand.

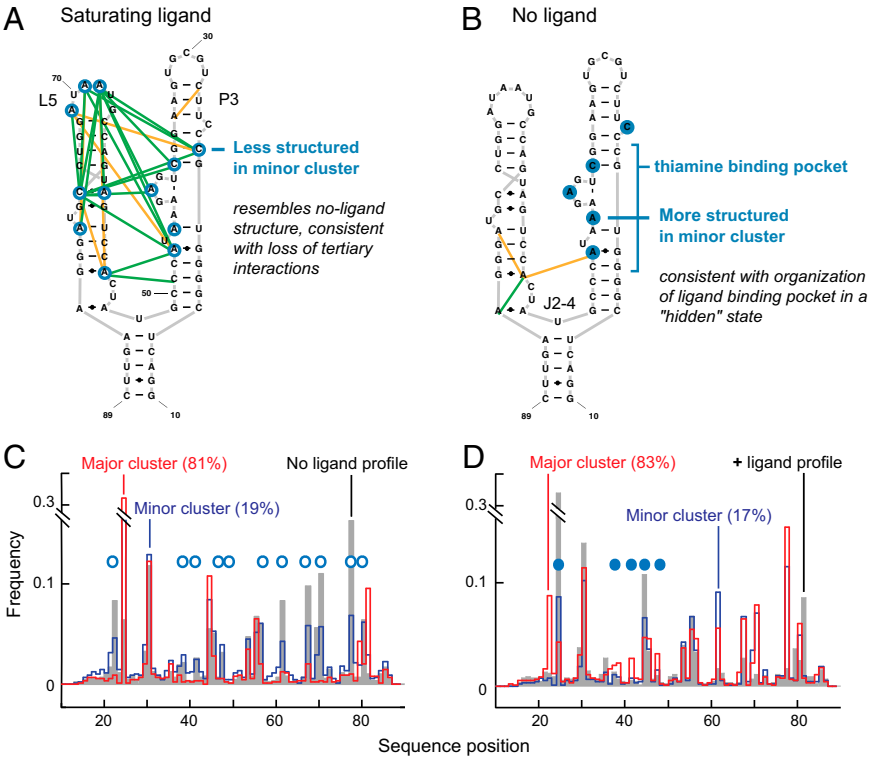

Fig. 5. RINGs and clustering analysis of the TPP riboswitch in the presence and absence of TPP ligand. RING analysis in the presence of (*A*) saturating ligand and (*B*) absence of ligand. Strong and moderate internucleotide associations are shown with green and yellow lines, respectively. Nucleotides that are less or more structured in the minor, less populated cluster are emphasized with open and closed spheres, respectively. Spectral clustering analysis in the (*C*) presence of saturating ligand and (*D*) absence of ligand. There are two clusters in each state. In the presence of saturating ligand, the major cluster (red) corresponds to the fully folded riboswitch. In the absence of ligand, the major cluster (red) reflects an unstructured state with few internucleotide interactions. The minor cluster (blue) in the saturating ligand sample is less structured than the major cluster and is similar to the no-ligand structure (gray). The minor cluster (blue) in the no-ligand sample is more highly structured than the major cluster specifically in the region of the thiamine binding pocket (blue closed circles).

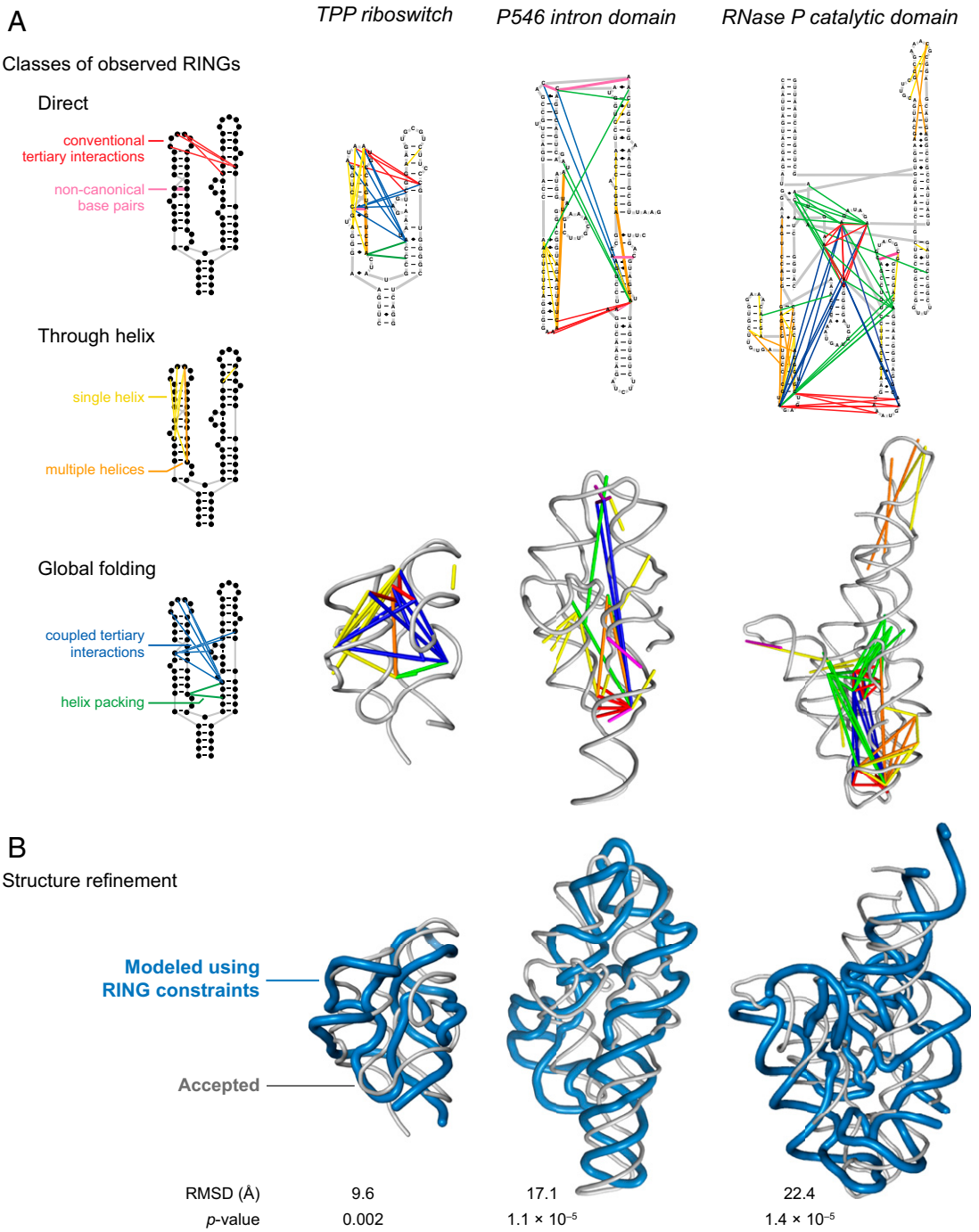

Fig. 6. Through-space RNA structural relationships revealed by RINGs. (*A*) Direct, through-helix, and global internucleotide interactions are illustrated on both secondary structures (*Upper*) and 3D models (7–9) (*Lower*). (*B*) Three-dimensional models determined for each RNA using RING interdependencies as constraints. The *P* values report the significance of each model (18); the secondary structure was input during refinement.

Finally, we examined the structure of the RNase P RNA as a function of Mg^{2+}. The networks of interactions were strikingly different in the presence and absence of Mg^{2+} (Fig. S5). The strong networks of interactions between L5 and L15.1 and in the structural core disappeared in the absence of Mg^{2+} and were replaced by interactions between P5.1 and P2 and within P7 (Fig. S5 *A* and *B*). Spectral clustering identified two clusters in the plus-Mg^{2+} state. The minor cluster in the plus-Mg^{2+} sample is distinct from both the fully folded RNA and from the no-Mg^{2+} structure (Fig. S5 *A* and *C*). Reactive nucleotides in the minor cluster comprise the L5–L15.1 and structural core interactions, indicating that these interactions are weakened in this state (Fig. S5*A*). Critically, single-molecule spectral clustering analysis shows that the TPP riboswitch and RNase P RNAs natively adopt multiple unique states, even under conditions generally assumed to promote formation of a single structure.

Principles of RNA Folding. RNA structure formation can be usefully approximated by assuming that stable helices, formed locally and stabilized by Watson–Crick pairing, are subsequently organized

into a 3D structure by longer-range tertiary interactions. RING analysis of the three RNAs studied here is consistent with this well-established structural hierarchy. For example, we observed RINGs that reflect noncanonical base pairs and loop–helix and loop–loop tertiary interactions that have been widely noted in prior structural studies (13, 14) (Fig. 6*A*, in magenta and red). RING analysis also identified interactions whose prevalence was previously not fully appreciated. Approximately one-third of all correlated interactions involve single-stranded or loop nucleotides at the opposite ends of individual helices. These through-helix interactions mean that structural communication in RNA can extend over long distances. In some cases, through-helix structural coupling extends through multiple stacked helices (Fig. 6*A*, in yellow and orange).

In addition, RING analysis indicates that tertiary interactions are not independent but instead are strongly dependent on other structural elements. We observed coupled interactions between well-defined individual tertiary structure motifs in both the TPP riboswitch and the P546 domain RNA (Fig. 6*A*, in blue). Disruption of any one tertiary interaction, by exclusion of ligand or by mutation, resulted in loss of the tertiary motif itself and also disrupted other interactions. RING data also support the importance of close helical packing. These interactions are especially obvious in the TPP riboswitch and in the structural core of the RNase P RNA (Fig. 6*A*, in green).

Analyses of the TPP riboswitch, the P546 domain, and the RNase P domain indicate that mutations (Fig. 4) or absence of ligand (Fig. 5 and Fig. S4) or divalent ions (Fig. 4*B* and Fig. S5) do not simply "subtract" an interaction from the structure but cause large-scale reorganization of RNA folding. None of the unfolded or less-folded states characterized was simply a less-structured version of a fully folded state. Instead, we find that less-structured states are stabilized by unique sets of interdependent interactions that, in general, have not been detected in prior ensemble or single-molecule studies.

Three-Dimensional RNA Structure Refinement. Because RING analysis identifies dense arrays of nucleotide interdependencies reflective of RNA tertiary structure, we explored whether these interactions could be used as restraints to model 3D RNA folds. A small number of constraints, reflective of through-space RNA structure, are often sufficient to yield high-quality structure models (15, 16). We used a two-step interaction potential (Fig. S6 *A*–*C*) to introduce free-energy bonuses when constituent nucleotides come into proximity during discrete molecular dynamics simulation (15–17). Introduction of RING constraints caused each RNA to preferentially sample collapsed states during the simulation (Fig. S6*D*). Following filtering by radius of gyration, representative structures were selected by hierarchical clustering. For each RNA characterized, we obtained high-quality and statistically significant (18) models (Fig. 6*B*) that correctly recapitulated the RNA architecture defined by high-resolution structures (7–9). For the RNase P RNA, we observed overlapping RINGs spanning two-thirds of the molecule and a second nonoverlapping set in P19 (Figs. 3*C* and 6*A*, *Right*); this suggests that the P3–P2–P19 element is not structurally linked to the rest of the RNA architecture. The accuracy of the 3D model for the RNase P RNA is especially high in the structural core (excluding the P3–P2–P19 element) with a 14.4 Å rmsd ($P < 10^{-6}$; Fig. S7) compared with the crystal structure. For the three RNAs studied here, the relative statistical significance of structure modeling actually increased with size, likely because a greater number of chemical modifications, and thus more nucleotide interactions, are detected with larger RNAs (Fig. 3*A*). RING–network interactions thus make possible both de novo identification of structural elements and modeling of folded domains for large RNAs (Fig. 6*B* and Fig. S7).

Perspective. Single-molecule structure analysis by correlated chemical probing, as detected by sequencing, represents a remarkably simple and generic approach for analysis of the global architectures of functionally important RNAs or DNAs. The fundamental insight that a single-molecule experiment can be created by simply recording multiple events in the same RNA or DNA strand is completely general and should inspire development of numerous new classes of experiments and biological discoveries. RING-MaP is unique in its simplicity and experimental concision and can be applied to virtually any biological RNA, without the requirement to introduce mutations, optimize for biophysical analysis, or introduce artificial structural probes. The single-molecule mutational profiling (MaP) approach described here using DMS can be readily extended to other RNA modification agents, to experiments that interrogate all four nucleotides simultaneously, to RNA–protein cross-linking, and to analysis of complex libraries of mutants. Single-molecule MaP experiments that explore protein–RNA, RNA–RNA, and DNA-mediated interactions simultaneously are clearly feasible. Higher-order structure is tightly linked to biological function. Thus, analogous to de novo discovery based on secondary structure characterization (6), identifying clusters of through-space RINGs in large RNAs and transcriptomes will enable widespread biological functional motif discovery.

Methods

Detailed descriptions of the RING-MaP approach, statistical association analysis, spectral clustering, and structure modeling are provided in the *SI Methods* and Figs. S8–S10. Processed data and software are freely available at the corresponding author's website (www.chem.unc.edu/rna). Sequencing data are available at the National Center for Biotechnology Information Sequence Read Archive.

ACKNOWLEDGMENTS. This work was supported by National Institutes of Health Grants AI068462 (for development of MaP technologies) and GM064803 (for three-dimensional structure modeling) (to K.M.W.).

1. Sharp PA (2009) The centrality of RNA. *Cell* 136(4):577–580.
2. Leontis NB, Lescoute A, Westhof E (2006) The building blocks and motifs of RNA architecture. *Curr Opin Struct Biol* 16(3):279–287.
3. Montange RK, Batey RT (2008) Riboswitches: Emerging themes in RNA structure and function. *Annu Rev Biophys* 37:117–133.
4. Dethoff EA, Chugh J, Mustoe AM, Al-Hashimi HM (2012) Functional complexity and regulation through RNA dynamics. *Nature* 482(7385):322–330.
5. Shendure J, Ji H (2008) Next-generation DNA sequencing. *Nat Biotechnol* 26(10):1135–1145.
6. Siegfried NA, Busan S, Rice GM, Nelson JAE, Weeks KM (2014) RNA motif discovery by SHAPE and mutational profiling (SHAPE-MaP). *Nat Methods* 11:959–965.
7. Serganov A, Polonskaia A, Phan AT, Breaker RR, Patel DJ (2006) Structural basis for gene regulation by a thiamine pyrophosphate-sensing riboswitch. *Nature* 441(7097):1167–1171.
8. Cate JH, et al. (1996) Crystal structure of a group I ribozyme domain: Principles of RNA packing. *Science* 273(5282):1678–1685.
9. Kazantsev AV, Krivenko AA, Pace NR (2009) Mapping metal-binding sites in the catalytic domain of bacterial RNase P RNA. *RNA* 15(2):266–276.
10. Murphy FL, Cech TR (1994) GAAA tetraloop and conserved bulge stabilize tertiary structure of a group I intron domain. *J Mol Biol* 236(1):49–63.
11. Szewczak AA, Cech TR (1997) An RNA internal loop acts as a hinge to facilitate ribozyme folding and catalysis. *RNA* 3(8):838–849.
12. Kulshina N, Edwards TE, Ferré-D'Amaré AR (2010) Thermodynamic analysis of ligand binding and ligand binding-induced tertiary structure formation by the thiamine pyrophosphate riboswitch. *RNA* 16(1):186–196.
13. Butcher SE, Pyle AM (2011) The molecular interactions that stabilize RNA tertiary structure: RNA motifs, patterns, and networks. *Acc Chem Res* 44(12):1302–1311.
14. Brion P, Westhof E (1997) Hierarchy and dynamics of RNA folding. *Annu Rev Biophys Biomol Struct* 26:113–137.
15. Gherghe CM, Leonard CW, Ding F, Dokholyan NV, Weeks KM (2009) Native-like RNA tertiary structures using a sequence-encoded cleavage agent and refinement by discrete molecular dynamics. *J Am Chem Soc* 131(7):2541–2546.
16. Lavender CA, Ding F, Dokholyan NV, Weeks KM (2010) Robust and generic RNA modeling using inferred constraints: A structure for the hepatitis C virus IRES pseudoknot domain. *Biochemistry* 49(24):4931–4933.
17. Ding F, et al. (2008) Ab initio RNA folding by discrete molecular dynamics: From structure prediction to folding mechanisms. *RNA* 14(6):1164–1173.
18. Hajdin CE, Ding F, Dokholyan NV, Weeks KM (2010) On the significance of an RNA tertiary structure prediction. *RNA* 16(7):1340–1349.